ELSEVIER

Coordination Chemistry Reviews
171 (1998) 287–307

COORDINATION CHEMISTRY REVIEWS

Photophysics of metal–organic π-conjugated polymers

K.D. Ley, K.S. Schanze *

Department of Chemistry, University of Florida, Gainesville, FL 32611-7200, USA

Received 7 July 1997; received in revised form 8 November 1997; accepted 19 November 1997

Contents

Abstract

A series of polyaryleneethynylene π-conjugated polymers that contain *fac*-(5,5′-diethynyl-2,2′-bipyridine)$Re^{I}(CO)_3Cl$ as part of the π-conjugated polymer backbone have been synthesized by Pd-mediated coupling chemistry. Three metal–organic polymers **P10**, **P25** and **P50**, have been prepared which contain, respectively, 10, 25 and 50 mol.% of the Re(I) repeat units in the polymer chain. These polymers have been characterized by ^{1}H- and ^{13}C-NMR and FTIR spectroscopy and gel permeation chromatography. The analysis indicate that the pholymers contain the intact Re(I) chromophore and M_n values of 10–15 kDa are typical (GPC, relative to polystyrene). The metal–organic polymers feature two spectrally-distinct absorption bands, one due to the π, π* absorption of the polymer backbone and another at lower energy which is attributed to the $d\pi(Re) \rightarrow \pi^*_{poly}$ metal to ligand charge transfer (MLCT) absorption. The luminescence properties of the polymers have been examined in fluid solution at 298 K and in a 2-methyltetrahedrofuran (MTHF) solvent glass at 77 K. These spectroscopic studies reveal that: (1) fluorescence from the $^{1}\pi, \pi^*$ exciton state is observed at 2.80 eV in all

* Corresponding author. E-mail: kschanze@chem.ufl.edu

PII S0010-8545(98)00016-2

of the polymers at 298 and 77 K, but the intensity and lifetime of the fluorescence is quenched as the mole fraction of Re in the polymers increases; (2) phosphorescence from the $^3\pi$, π^* state of the conjugated polymer backbone is observed at 1.93 eV in **P10–P50** at 77 K; (3) luminescence from the $d\pi \rightarrow \pi^*$ MLCT state is observed at 1.8 eV in the metal–organic polymers at 77 K. © 1998 Elsevier Science S.A.

Keywords: π-Conjugated polymers; Fluorescence; Phosphorescence; Luminescence

1. Introduction

π-Conjugated polymers, typified by poly-p-phenylene (PPP), polyphenylene vinylene (PPV), and polyphenylene ethynylene (PPE), represent a class of organic based materials that possess unique optical and electronic properties [1]. Some examples of these unique properties include high electronic conductivity in the doped polymers [2], high absorptivity in the visible and/or near-IR regions [3] and large fluorescence quantum yields [4]. In addition to the useful optical and electronic properties, the fact that the materials are organic in nature makes it possible to readily process them into films that display the favorable mechanical properties characteristic of organic polymers. Because of this unique combination of properties, π-conjugated polymers have received considerable attention from scientists and engineers interested in fabricating electronic and/or electro-optical devices which consist partly or wholly of π-conjugated polymers [5–7]. One significant example of a device application for π-conjugated polymers is as the active medium for wavelength-tunable, organic-based light emitting diodes (LEDs) [8–11].

In part, because of the significant potential for commercially viable applications [12], π-conjugated polymers have become the subject of intense research by chemists and physicists. In particular, a number of recent studies have examined the photophysical properties of organic-based π-conjugated polymers in an effort to provide a clear basis for understanding and controlling the light absorption and emission properties of the materials [13–20]. Most of this work has focused on PPV and its analogs, since this material is currently the most promising candidate for use in organic LEDs.

Although significant research attention has focused on all-organic polymers, relatively little work has been carried out concerning the photophysical properties of π-conjugated polymers that contain transition metal complexes [21–24]. This is surprising, given that the photophysics and excited state redox properties of many transition metal chromophores are tunable [25–27], and that this feature could be very useful in allowing one to tailor the photophysical properties of π-conjugated polymers. Recognizing the void in this area, we recently set out to synthesize and characterize the photophysics of π-conjugated polymers that contain transition metal chromophores as an integral component of the π-conjugated backbone [28]. In our initial foray into this area, we prepared and characterized the series of π-conjugated polymers **P0–P50**. The structure of these polymers is based on the polyaryleneethynylene (PPE) architecture and they contain the *fac*-(bpy)$Re^{I}(CO)_3Cl$ chromophore as an integral component of the π-conjugated backbone.

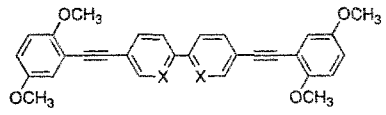

1 : X = C-H
2 : X = N

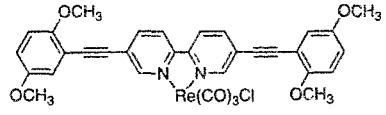

3

Scheme 1. Chemical structures of model compounds

The Re(I) chromophore was selected for incorporation into the PPE-type π-conjugated polymers for several reasons. First, this chromophore features an energetically low-lying metal to ligand charge transfer (MLCT) excited state based on a dπ (Re)→π* (diimine) transition [27,29]. The MLCT state has been thoroughly studied in an array of (diimine)$Re^{I}(CO)_3X$ complexes and usually it is long-lived and luminesces in the red part of the visible spectrum [27,29,30]. Second, the MLCT excited state of the Re(I) chromophore is a moderately strong oxidant, and therefore, polymers that contain this chromophore may display unusual photoredox (or photoconductive) properties [27]. Third, the (bpy)$Re^{I}(CO)_3Cl$ complex carries a neutral charge; consequently, the Re(I) containing polymers are electrically neutral and are very soluble in low-dielectric solvents such as $CHCl_3$ and THF.

The present manuscript describes the synthesis and photophysical characterization of polymers **P0–P50**. In addition, the small molecule model compounds **1–3** (Scheme 1) have also been examined to provide information concerning the properties of the isolated chromophoric units which comprise the polymer. The studies indicate that Pd-mediated coupling chemistry [31,32] can be used to incorporate the diethynylbipyridine-substituted Re(I) metal complex into the backbone of PPE-type π-conjugated polymers. The photophysics of the resulting π-conjugated metal–organic polymers is unusual in that the materials display the spectroscopic signatures of both the organic-based π-conjugated network and the metal-based charge transfer states.

2. Results and discussion

2.1. Synthesis of model compounds and conjugated polymers

Schemes 2–4illustrate the overall synthetic route used to prepare model compounds **1–3** and polymers **P0–P50**. The key compound in these schemes is 5,5′-diethynyl-2,2′-bipyridine (**5**), which is obtained in high yield from 5,5′-dibromo-2,2′-bipyridine (**4**) by treatment with trimethylsilyl acetylene in the presence of the

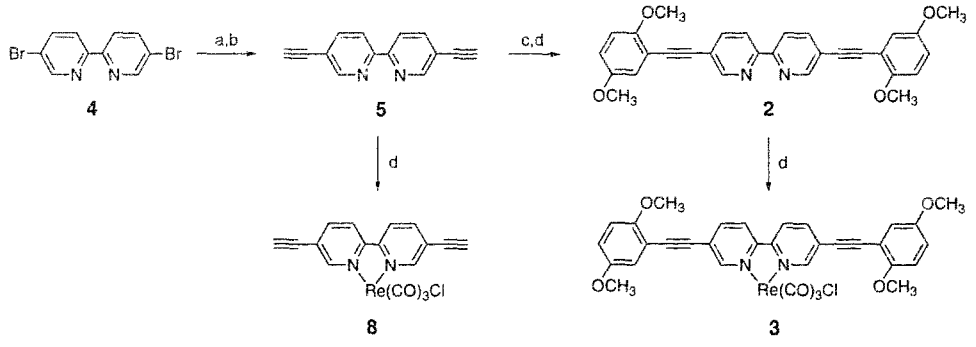

a) TMS-≡-H, $Pd(PPh_3)_2Cl_2$, CuI, THF, i-Pr_2NH; b) KOH; c) 2-iodo-1,4-dimethoxybenzene, $Pd(PPh_3)_2Cl_2$, CuI, THF, i-Pr_2NH; d) $Re(CO)_5Cl$, reflux.

Scheme 2. Synthesis of Re(I) complexes

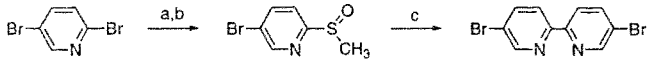

a) CH_3SNa, DMF; b) H_2O_2, HOAc; c) n-PrMgBr, THF, Et_2O.

Scheme 3. Synthesis of dibromopyridine

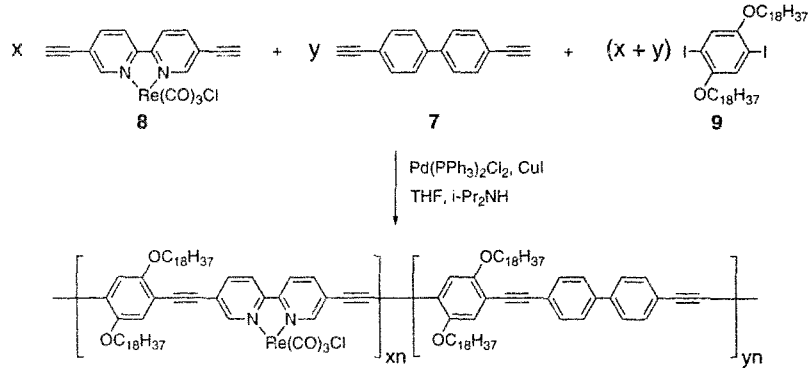

P0 : x = 0, y = 1.0 **P25** : x = 0.25, y = 0.75
P10 : x = 0.1, y = 0.9 **P50** : x = 0.5, y = 0.5

Scheme 4. Polymer synthesis and structure

$Pd(PPh_3)_2Cl_2$ catalyst [33]. Synthesis of dibromobipyridine **4** via treatment of 2,2′-bipyridine · HBr with Br_2 at high temperature under pressure has been reported by Ziessel and coworkers [34], but in our hands this procedure proved to be very time-consuming and produced **4** in low yield. Thus, in order to improve access to the key compound **5**, we developed a new synthesis of **4**, which is a modification of the synthesis of 5,5′-dichloro-2,2′-bipyridine [35]. This procedure is outlined in Scheme 3

and affords **4** in three steps with an overall 40% yield from the commercially available starting compound, 2,5-dibromopyridine.

Once diethynylbipyridine **5** was available in a sufficient quantity, synthesis of the model compounds and polymers proceeded at a rapid pace. Thus, treatment of **5** with two equivalents of 2-iodo-1,4-dimethyoxybenzene [6] in the presence of $Pd(PPh_3)_4$ afforded dimethoxyphenylethynyl bipyridine (**2**) in good yield. Treatment of ligand **2** with one equivalent of $Re(CO)_5Cl$ in refluxing toluene/CH_2Cl_2 produced model complex **3** which has been fully characterized by NMR, FAB-MS as well as various photophysical techniques.

Polymers **P0–P50** were prepared via Pd-mediated cross coupling as illustrated in Scheme 4. [13,14] The polymers differ with respect to the mole ratio of 4,4′-diethynylbiphenyl (**7**) and (5,5′-diethynyl-2,2′-bipyridine)$Re^{I}(CO)_3Cl$ (**8**) used in the polymerization reaction mixture. (In the acronym used to identify the polymers, **Pn**, the number indicates the mol.% of **8** used in the reaction mixture. For example, in the synthesis of **P10**, the reaction mixture contained 90 mol.% of **7** and 10 mol.% of **8**.) Polymerization was effected under various reaction conditions using several different Pd catalysts including $Pd(PPh_3)_2Cl_2$, $Pd(dba)_2$ and $Pd(PPh_3)_4$. Optimal results were obtained with 5 mol.% $Pd(PPh_3)_2Cl_2$ and 5 mol.% CuI catalyst in the THF/diisopropylamine (2:1 v:v) at 70° for 16 h. The polymers were analyzed by ^1H- and ^{13}C-NMR spectroscopy, as well as FTIR, UV-visible absorption, and fluorescence spectroscopy (see below).

2.2. Polymer characterization

An important objective of the present investigation has been the structural characterization of metal containing polymers **P0–P50**. The structural characterization was effected on a series of polymers synthesized under identical conditions, the only variable being the mole fraction of the Re-containing diethynyl monomer (**8**) used in the reaction mixture. The resulting series of polymers **P0–P50** were characterized by using gel permeation chromatography (GPC), ^1H- and ^{13}C-NMR and FTIR spectroscopy. In the present report we describe in some detail the results of the GPC and FTIR analysis, while the NMR results will be described elsewhere.

The GPC method used to characterize **P0–P50** relies on polystyrene standards to provide information regarding the molecular weight distribution of the polymer sample. Unfortunately, owing to the significant structural differences between polymers **P0–P50** and polystyrene (e.g. **P0–P50** are rigid-rod polymers, while polystyrene is a random coil), molecular weight distributions determined by GPC do not provide information regarding the absolute molecular weight of the polymers [36]. Despite this shortcoming, GPC data is useful in several ways. First, it provides a measure of the relative molecular weight distributions of a series of related polymers and, second, it allows one to determine the dispersion in the molecular weight distribution of a given polymer sample. The dispersion is described by the polydispersity index (PDI) which is given by the ratio M_w/M_n, where M_w and M_n are, respectively, the weight- and number-average molecular weights of the sample [37].

GPC traces for analysis of **P0–P50** are illustrated in Fig. 1 and the results of the GPC analysis are listed in Table 1. Several points are clear upon inspection of the

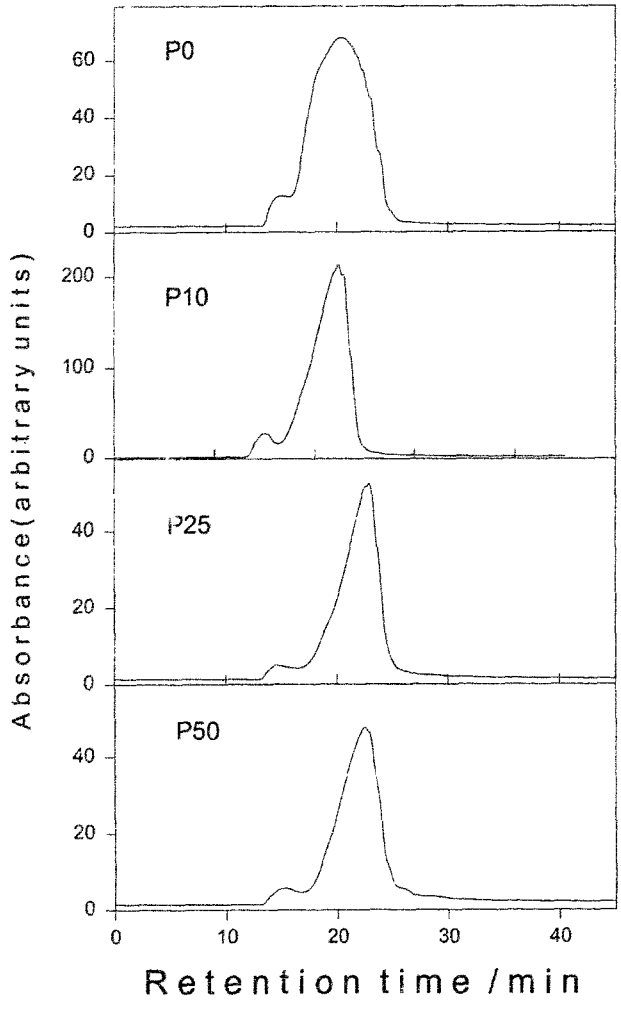

Fig. 1. GPC chromatogram traces for polymer samples **P0–P50**.

Table 1
GPC analysis of polymers[a]

Polymer	100% of chromatogram area			95% of chromatogram area		
	M_n (kD)	M_w (kD)	PDI	M_n (kD)[b]	M_w (kD)	PDI
P0	15.2	79.7	5.2	13.5	37.4	2.7
P10	10.5	67.9	6.4	8.8	20.7	2.3
P25	8.9	69.2	7.7	7.9	16.4	2.1
P50	6.3	56.8	8.8	7.8	16.0	2.0

[a]THF solvent relative to polystyrene standards.
[b]Author please supply relevant caption.

GPC data. First, each polymer sample is characterized by a bimodal molecular weight distribution. The polymers are dominated by a single fraction ($\approx$95% chromatogram area) which has M_n ranging from 8–14 kD. However, each sample also exhibits a small high molecular weight fraction ($\approx$5% chromatogram area, $M_n > 100$ kD). This bimodal distribution is consistently observed, and apparently is characteristic of the methodology used to produce the "hairy rod" polyaryleneethynylene polymers. One possibility is that the high-M_w fraction is due to cross-linked polymer chains that are formed by side reactions produced by the PdL_2 catalyst. A second possibility is that the high-M_w fraction is component of the sample that is physically cross-linked by entanglement of the octadecyl side-chains. Table 1 contains listings of the M_w, M_n and PDI values determined for the polymer samples by using the entire chromatogram area and by using the area under the principal eluting fraction. This comparison clearly illustrates that the PDI and M_w values are skewed upward significantly by the presence of the small, high molecular weight fraction. However, note that the M_n value, which better represents the composition of the bulk of the polymer sample (on a per mole basis), is not influenced significantly by the high molecular weight fraction. The next point that is evident from the GPC data is that the M_n values for the metal–organic polymers (e.g. **P10–P50**) are generally lower compared to that for the organic polymer **P0**. The lower M_n values for the metal-containing polymers likely reflect the fact that Re-bipyridine monomer **8** is less reactive in the Pd-catalyzed cross coupling reaction compared with the biphenyl monomer **7**. The impact that this difference in reactivity has on the structure of the polymers is unclear at present. However, if **8** is incorporated into the growing polymer chains more slowly than **7**, it is likely that the Re sites are dispersed within a polymer that is primarily organic, as opposed to being contained in segments dominated by Re-containing repeat units.

While it is not possible to make any definitive conclusions regarding the actual molecular weight of **P0–P50**, comparison of the GPC data for the present polymers with that reported for structurally similar PPE-type rigid rod polymers implies that polymer samples **P0–P50** are likely to consist of chains having 10–30 repeat units [36]. Ongoing studies in our laboratory seek to use ^{1}H-NMR analysis of p-*tert*-butylphenyl end-capped polymers to determine the degree of polymerization (X_n) for the metal containing polymers, but these experiments have been frustrated due to overlap between the resonance of the *tert*-butyl end-cap group and the very strong resonance of the octadecyl polymer side-chains.

The carbonyl groups within the (bpy)$Re^I(CO)_3Cl$ chromophore typically give rise to three clearly resolved IR bands in the 1900–2050 cm^{-1} region [38]. FTIR analysis of polymers **P10–P50** in CCl_4 solution confirms the presence of the intact Re(I) chromophore by the appearance of CO bands at 2024, 1930 and 1907 cm^{-1} [the a′(1), a″ and a′(2) bands, respectively]. The approximate molar absorptivity for the a′(1) band in the (bpy)$Re(CO)_3Cl$ chromophore was determined by examining the concentration dependence of the 2024 cm^{-1} FTIR absorption of (4,4′-(di-*tert*-butyl)-2,2′-bipyridine)$Re(CO)_3Cl$ in CCl_4 ($\epsilon \approx 5000\ M^{-1}\ cm^{-1}$). By using this value it is possible to estimate the concentration of the (bpy)$Re(CO)_3Cl$ chromophore present in solutions of polymers **P10–P50**. This information, in turn

allows us to estimate the mole fraction of the (bpy)Re(CO)$_3$Cl repeat unit (χ_{Re}) in the polymers. This analysis leads to values of $\chi_{Re}=0.13$, 0.16 and 0.33, respectively, for **P10**, **P25** and **P50**.

2.3. Photophysics of model compounds

The photophysics of model compounds **1–3** were investigated to define the properties of the chromophoric units that comprise the metal–organic π-conjugated polymers. Table 2 contains a listing of many photophysical parameters for the compounds, including absorption maxima and extinction coefficients, as well as emission maxima, quantum yields and lifetimes. Fig. 2 compares the absorption and emission spectra of the three compounds at ambient temperature in THF solution and Fig. 3(a) compares the emission spectra of **1** and **2** at 77 K in a 2-methyltetrahydrofuran (MTHF) solvent glass.

Organic compounds **1** and **2** display qualitatively similar absorption and fluorescence properties. The absorption of both chromophores is dominated by a comparatively intense near-UV transition which is due to the lowest π, π* transition. In fluid solution, both compounds emit strong blue fluorescence ($\Phi_{fl}\approx 1.0$) with a small Stokes shift, which is presumably due to the comparatively rigid structure of the compounds. The absorption and fluorescence maxima of bipyridine **2** are red-shifted slightly relative to those for biphenyl **1**, apparently due to the effect of the bipyridyl nitrogens on the HOMO-LUMO gap. The fluorescence lifetimes of **1** and **2** are on the order of 1 ns, which is typical for π, π* fluorescence [39]. The large fluorescence quantum yields coupled with the short lifetimes indicate that the radiative decay rates of both chromophores are very large ($k_r\approx 10^9\ s^{-1}$). The low temperature fluorescence spectra of **1** and **2** [Fig. 3(a)] are unremarkable. The spectra are blue-shifted compared with the room temperature spectra and vibronic structure is observed. Phosphorescence was not detected in the low-temperature spectra of **1** and **2** for $\lambda<800$ nm.

Table 2
Photophysical properties of model compounds[a]

Compound	λ_{max} absorbance (nm) (ϵ_{max} $M^{-1}cm^{-1}10^3$)	Assignment	λ_{max} emission (nm)298 K	Φ_{em} 298 K	τ_{em} (ns) 298 K	λ_{max} emission (nm)[b]77 K
1	314 (sh)(40.0)	π, π*	413	0.95	1.1	389
	342 (52.5)	π, π*				
2	330 (40.5)	π, π*	470	0.94	2.4	413
	366 (56.5)	π, π*				
3	406 (10.1)	π, π* IL & MLCT	433 (IL)	<0.001	<1 ns (IL)	410
	322 (10.3)	π, π* IL & MLCT	690 (MLCT)		90 ns (MLCT)	590

[a]Ambient temperature data for THF solutions and low-temperature data in 2-methyltetrahydrofuran (MTHF) glass.
[b]0-0 band in structured low-temperature spectrum.

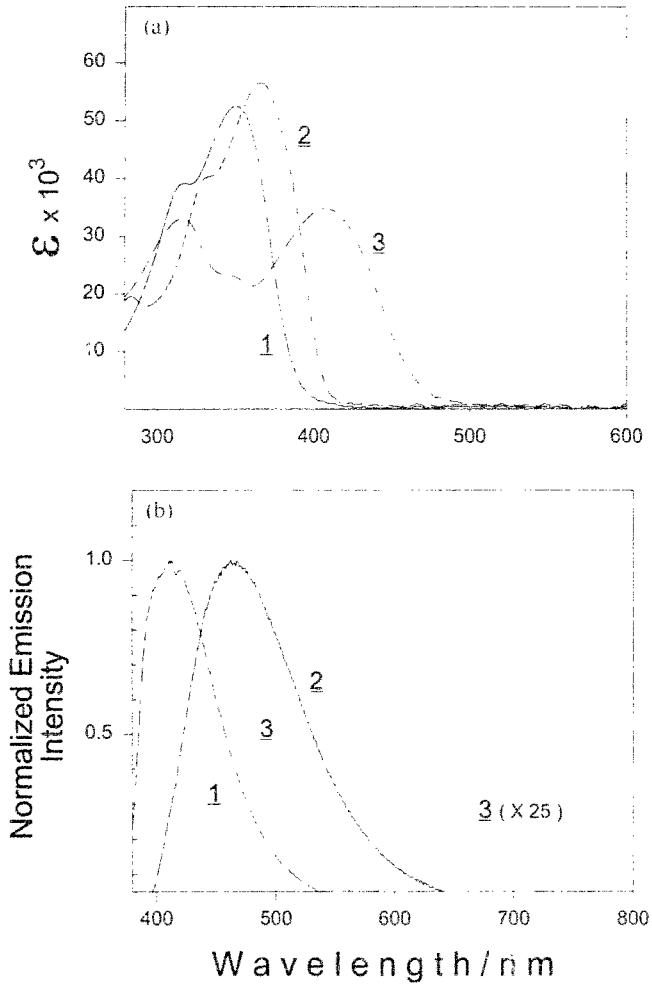

Fig. 2. (a) UV-visible absorption spectra of model compounds **1**–**3** in THF solution. Solid line, **1**; dashed line, **2**; dash–dot line, **3**. (b) Luminescence spectra of model compounds **1**–**3** in THF solution at 298 K. Dashed line, **1**; solid line, **2**; dotted line, **3**.

The absorption and luminescence properties of Re(I)model complex **3** differ significantly compared with those of the free bipyridine ligand **2**. First, the absorption spectrum [Fig. 2(a)] is dominated by a broad band with $\lambda_{max} \approx 406$ nm. This band is red-shifted and has a significantly lower molar absorptivity compared with the π, π^* absorption of free ligand **2**. Complexes of the type (diimine)$Re^{I}(CO)_3Cl$ typically feature a low-energy absorption ($\epsilon \approx 5.0 \times 10^3\ M^{-1}\ cm^{-1}$) due to the $d\pi(Re) \rightarrow \pi^*$ (diimine) MLCT transition [27,29]. On this basis, we assign the 406 nm absorption in **3** to the MLCT transition. However, note that the molar absorptivity of the 406 nm band in **3** is larger than typical for MLCT transitions in related complexes, and this implies that the low energy band may also have some π, π^* intraligand (IL) character.

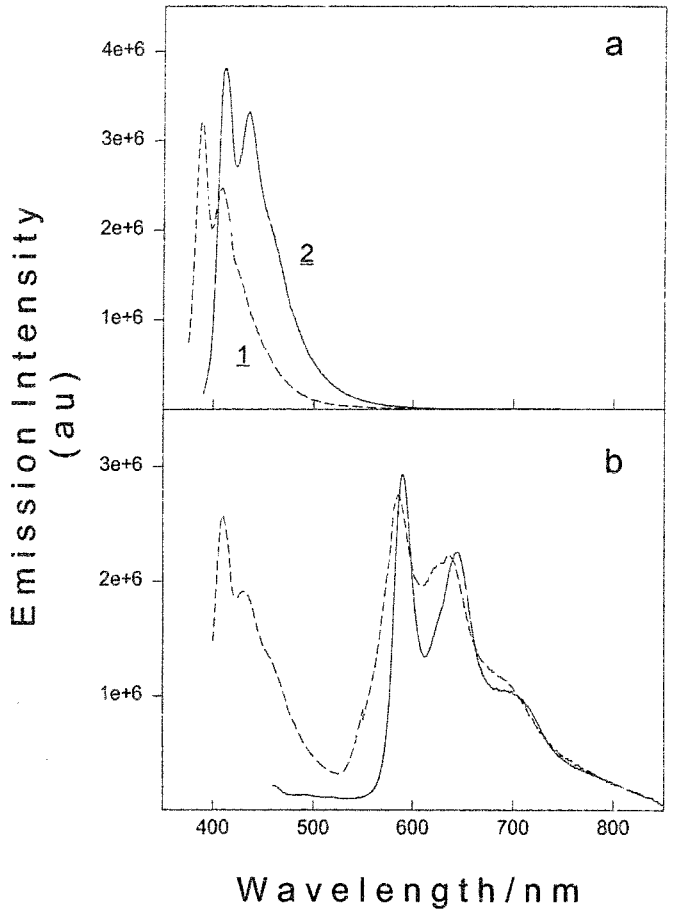

Fig. 3. (a) Luminescence spectra at 77 K in MTHF solvent glass. (a) Dashed line, **1** ($\lambda_{ex}=350$ nm); solid line, **2** ($\lambda_{ex}=350$ nm). (b) Dashed line, **3** ($\lambda_{ex}=380$ nm); solid line, **3** ($\lambda_{ex}=450$ nm).

Fig. 2(b) displays the room temperature emission spectrum of **3** obtained with $\lambda_{ex}=380$ nm. First, it is important to note that although two emission bands are observed, the quantum yields of the emissions are very weak (Table 2). The emission spectrum is dominated by a relatively narrow band at $\lambda_{max}=433$ nm. The lifetime of the 433 nm emission is very short (<1 ns), and on this basis we assign it to fluorescence from the $^1\pi$, π^* IL state of the coordinated bipyridine ligand. The low quantum yield and short lifetime of the π, π^* IL fluorescence arises because the IL state is quenched by fast intramolecular energy transfer to the MLCT manifold, which is at a lower energy (vide infra). Fluorescence from π, π^* IL state is not typically observed in transition metal complexes; however, in **3** the large radiative decay rate of the diphenylethynylbipyridine ligand allows fluorescence to "leak out" even though the π, π^* state is short-lived. Interestingly, the π, π^* IL fluorescence is blue-shifted relative to the position of the fluorescence of the free bipyridine ligand **2**. The blue shift (and vibronic shoulder) in the π, π^* IL fluorescence is likely due

to the fact that the chelated ligand is unable to relax along the inter-ring torsional mode after photoexcitation. In addition to π, π* IL fluorescence, **3** features a very weak, broad emission with $\lambda_{max} \approx 690$ nm and $\tau \approx 90$ ns. The characteristics of this emission strongly suggest that it can be assigned to the MLCT excited state.

Fig. 3(b) illustrates two emission spectra of Re(I) complex **3** at 77 K in MTHF, one collected with $\lambda_{ex} = 380$ nm and the second with $\lambda_{ex} = 450$ nm. The spectrum obtained with the shorter excitation wavelength shows two structured emission bands: one with $\lambda_{max} \approx 410$ nm and the second with $\lambda_{max} \approx 590$ nm. The spectrum obtained with the longer excitation wavelength features only the long wavelength emission. First, it is clear that the 410 nm emission band is due to fluorescence from the $^1\pi$, π* IL state of the diethynylbipyridine ligand. This assignment is supported by the fact that the position and bandshape of this band is closely similar to that observed for free ligand **2** at 77 K [see Fig. 3(a)]. Assignment of the long-wavelength luminescence band is more dubious. A curious feature is that the bandshape of this emission is subtly different for 380 and 450 nm excitation. In particular, with 450 nm excitation the band features three very clearly resolved vibronic transitions. By contrast, with 380 nm excitation, the resolution of the vibronic bands is poorer, and there is evidence for an underlying band on the 0.1 transition. Given this excitation wavelength dependence, we believe that the long-wavelength emission band is due to a superposition of phosphorescence from the $^3\pi$, π* IL state and to luminescence from the dπ→π* MLCT state. Assuming that MLCT state contributes to the long-wavelength emission, then the MLCT emission is blue-shifted approximately 2500 cm^{-1} compared with its position at 298 K (e.g. the band shifts from 690 to 590 nm upon cooling). Such blue-shifts are characteristic for MLCT emission upon cooling to 77 K, and the 2500 cm^{-1} shift observed for **3** is typical [40,41].

2.4. Polymer photophysics

The absorption spectra of **P0–P50** are compared in Fig. 4(a). The polymers feature an absorption band ($\lambda_{max} \approx 400$ nm) having an intensity that decreases with increasing χ_{Re}. This absorption band is similar in energy and bandwidth to the absorption of structurally-related PPE-type polymers [13–16], and on this basis it is assigned to the π, π* transition of the conjugated polymer backbone. The Re-containing polymers **P10–P50** feature an additional absorption band ($\lambda = 440$–540 nm) with an intensity that increases with χ_{Re}. This long wavelength absorption is clearly associated with the (bpy)$Re(CO)_3Cl$ chromophore and it is assigned to the MLCT transition arising from promotion of an electron from a dπ (Re) level into a π* level of the conjugated polymer backbone (e.g. $d\pi \rightarrow \pi^*_{poly}$ MLCT). Note that the MLCT transition in the polymers is red-shifted significantly from its position in model complex **3**. The red-shift likely arises because the π^*_{poly} orbital (which is the acceptor for the MLCT transition) is significantly delocalized (and therefore stabilized) by the conjugated polymer backbone.

Excitation of solutions of **P0–P50** into the π, π* absorption band produces a strong emission with $\lambda_{max} \approx 435$ nm and a shoulder on the long-wavelength side due to vibronic coupling [Fig. 4(b)]. The emission is Stokes-shifted only a small extent

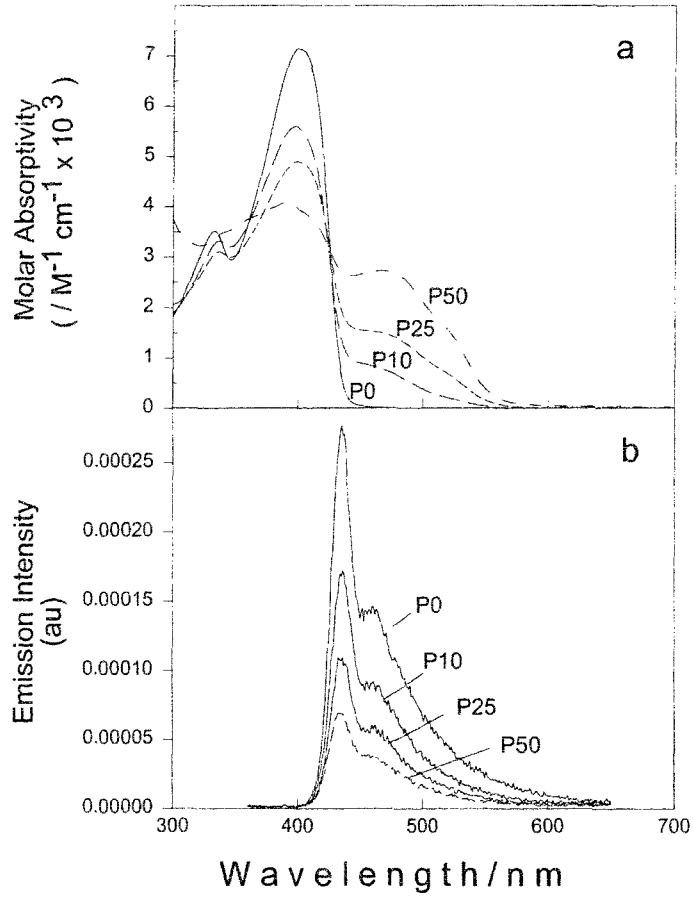

Fig. 4. (a) Absorption spectra of polymers **P0–P50** in THF solution. Spectra were obtained on solutions having the same polymer concentration (mass per unit volume). Spectra are converted to a "molar absorptivity" scale by dividing the concentration by the median molecular weight of the monomer repeat units. (b) Fluorescence spectra of **P0–P50** in at 298 K ($\lambda_{ex}=380$ nm). Spectra are normalized to reflect the fluorescence quantum yields.

from the π, π* absorption of the polymer backbone, and on this basis it is assigned to fluorescence from the $^1\pi$, π* exciton state. The $^1\pi$, π* assignment is supported by the fact that the fluorescence is very similar in energy and bandshape to that observed in related PPE- and PPV-type π-conjugated polymers [4,13–20].

Fluorescence quantum yields (Φ_{fl}) were determined for **P0–P50** and the results are listed in Table 3. In general, Φ_{fl} is comparatively large for all of the polymers; however, it is apparent that Φ_{fl} decreases as χ_{Re} increases. The fluorescence decay kinetics for solutions of **P0–P50** (Table 3) are biexponential but are generally dominated by a large amplitude component with a lifetime of less than 1 ns. In order to facilitate comparison of the overall fluorescence decay kinetics of the different polymers, median lifetimes were computed according to the expression, $\langle\tau\rangle=\alpha_1\tau_1+\alpha_2\tau_2$, where α_i and τ_i, are, respectively, the normalized amplitude and

Table 3
Photophysics of polymers[a]

Polymer	λ_{max} absorbance (nm)298 K	Assignment	λ_{max} emission (nm)298 K	Φ_{fl}^{b} 298 K	τ_i (ns) (α_i)[c] 298 K	$\langle\tau\rangle$ (ns)[d] 298 K	λ_{max} emission (nm)77 K
P0	400	π, π*	435	0.28	0.81 (0.95) 6.39 (0.05)	1.1	443
P10	400 465 (sh)	π, π* dπ→π* MLCT	435	0.16	0.72 (0.96) 2.19 (0.04)	0.78	443 643 ≈690
P25	400 469 (sh)	π, π* dπ→π* MLCT	435	0.11	0.32 (0.81) 1.04 (0.19)	0.48	443 643 ≈690
P50	388 469	π, π* dπ→π* MLCT	432	0.073	0.12 (0.46) 0.62 (0.54	0.40	434 643 ≈690

[a]Ambient temperature data for THF solutions and low-temperature data in 2-methyltetrahydrofuran (MTHF) glass.
[b]Quantum yield of π, π* fluorescence.
[c]Lifetime (τ_1) and normalized amplitude (α_1) recovered from fit of π, π* fluorescence decay to biexponential expression, $I(t)=\alpha_1 \exp\{-t/\tau_1\}+\alpha_2 \exp\{-t/\tau_2\}$.
[d]Median lifetime calculated from the expression, $\langle\tau\rangle=\alpha_1\tau_1+\alpha_2\tau_2$.

lifetime of the ith decay component recovered from the biexponential fits of the decays ($\langle\tau\rangle$, Table 3). Interestingly, the median fluorescence lifetimes for **P0–P50** (like the fluorescence quantum yields) decrease as χ_{Re} increases. The parallel decrease in $\langle\tau\rangle$ and Φ_{fl} with increasing ξ_{Re} indicates that the $^1\pi$, π* exciton is quenched by the (bpy)$Re^{I}(CO)_3Cl$ chromophore in the polymers. However, although quenching is observed, it is not particularly efficient even at high χ_{Re}.

Further information regarding the excited states involved in the photophysics of **P0–P50** comes from luminescence spectroscopy carried out at 77 K in MTHF solvent glasses. Fig. 5 illustrates low temperature emission spectra of **P10–P50** obtained with excitation into the π, π* manifold of the π-conjugated polymer ($\lambda_{ex}=380$ nm). First, at low temperature all of the polymer samples (including P0) exhibit fluorescence from the $^1\pi$, π* state of the polymer backbone. Remarkably, the fluorescence band maximum and bandwidth is almost the same at room temperature in fluid and at low temperature in the glass [compare Figs. 4(b) and 5]. This correspondence reveals very weak electron–phonon coupling in the fluorescent exciton state and implies that the exciton is very delocalized. At low temperature metal–organic polymers **P10–P50** exhibit additional emission band(s) in the red. This emission appears as a sharp band with $\lambda_{max}\approx 643$ nm (fwhm ≈ 400 cm^{-1}) superimposed on a broad band with $\lambda_{max}\approx 690$ nm. We tentatively assign the sharp 643 nm luminescence feature to phosphorescence from the $^3\pi$, π* state of the conjugated

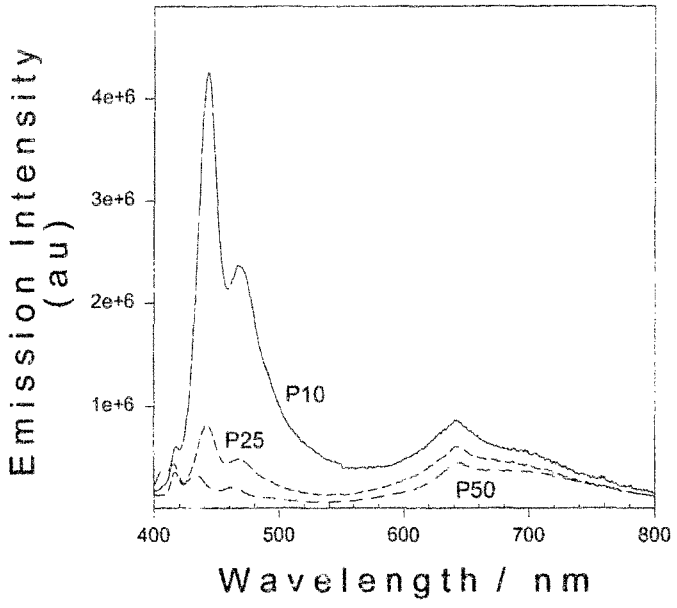

Fig. 5. Luminescence spectra of polymers **P10–P50** in MTHF glass at 77 K ($\lambda_{ex}=380$ nm). Spectra were obtained on samples having equivalent concentration (mass per unit volume). Because of the sample and cryostat configuration it was difficult to maintain consistent sample position; therefore, relative emission intensities are only approximate. Small peaks in 400–410 nm region are due to Raman scattering.

polymer backbone and the broad 690 nm emission to the $d\pi$ (Re)$\rightarrow\pi^*_{poly}$ MLCT manifold.

Although phosphorescence has previously not been observed in many π-conjugated polymer systems, our assignment is supported by the close similarity between the 643 nm luminescence and that observed from metal–organic PPE polymer **10** (Scheme 5) [42]. Thus, at 25 K **10** exhibits fluorescence at 405 nm (3.06 eV) and phosphorescence at 521 nm (2.38 eV, fwhm $\approx 320\ cm^{-1}$); these spectral assignments indicate that in **10** the singlet–triplet (S–T) splitting is approximately 0.7 eV. Two points are significant when comparing the luminescence of **P10–P50** and **10**. First, the width of the 0–0 phosphorescence band in **10** is $320\ cm^{-1}$, in good agreement with the width of the 643 nm feature in **P10–P50**. Second, assuming that in **P10–P50** the 443 nm (2.80 eV) emission is fluorescence and the 643 nm (1.93 eV) emission is phosphorescence, a 0.8 eV S–T splitting is computed, in close agreement with the S–T splitting for **10**.

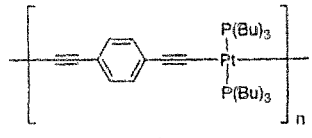

10

Scheme 5. Structure of organometallic polymer.

At this point the MLCT assignment for the broad luminescence band underlying the $^3\pi$, π^* phosphorescence is less solid. However, assuming that the MLCT assignment is correct, then the low temperature emission spectra imply that the energy of the MLCT state in the polymers ($\lambda_{max}=690$ nm, 1.8 eV) is approximately 0.3 eV lower in energy than in model complex **3** ($\lambda_{max}=590$ nm, 2.1 eV). This difference in MLCT states energies derived from the low temperature emission spectra is at least consistent with the difference in the position of the MLCT absorption bands of **3** ($\lambda_{max}=406$ nm, 3.05 eV) and the polymers ($\lambda_{max}\approx460$ nm, 2.70 eV).

2.5. *Excited states in the metal containing polymers*

Based on the spectroscopic assignments for the absorption and luminescence data it is possible to construct a Jablonski diagram (Fig. 6). In this diagram, states arising from the organic component of the polymer are at left, while states arising from the metal-containing repeat units are given at right. The state energies are based on the position of luminescence bands (E_{max}) in the low temperature spectra, except for the ^{1}MLCT level which is based on the absorption band maximum. Thus, the $^1\pi$, π^* and $^3\pi$, π^* exciton states of the π-conjugated polymer backbone lie at 2.80 and 1.94 eV, respectively, while the ^{1}MLCT and ^{3}MLCT levels arising from the $d\pi\rightarrow\pi^*_{poly}$ transition lie at 2.7 and 1.8 eV, respectively. Excitation spectroscopy (data not presented) implies that energy transfer occurs from the $^1\pi$, π^* exciton to the $d\pi\rightarrow\pi^*_{poly}$ ^{3}MLCT manifold, as anticipated based on the relative ordering of the

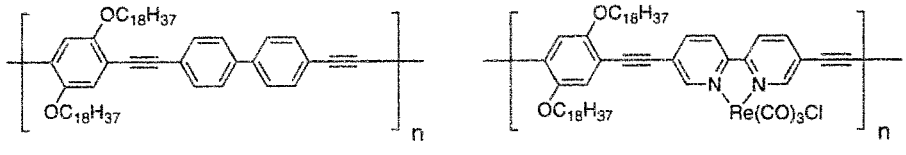

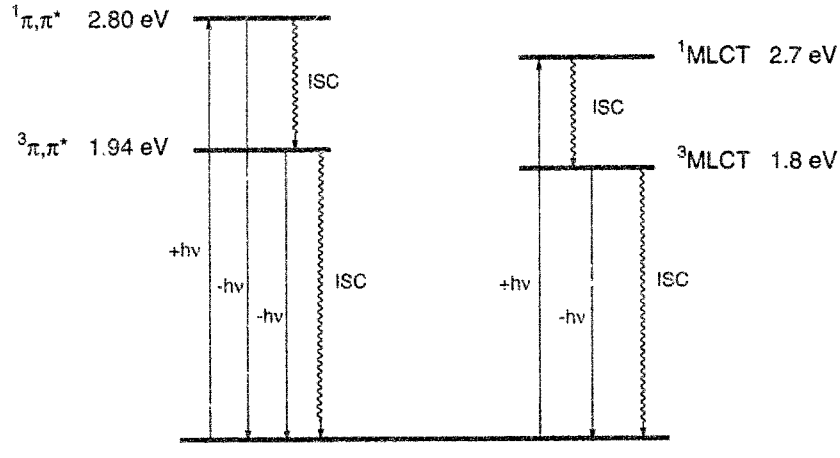

Fig. 6. Jablonski diagram for polymers **P10–P50**.

states. On the other hand, the low temperature spectroscopy implies that the $^3\pi, \pi^*$ exciton and the ^{3}MLCT state are in close energetic proximity. Furthermore, the apparent observation of emission from both states at low temperature implies that the two states are either in equilibrium or are not rapidly interconverting. Recent studies of d^6 metal complexes indicate that a barrier to interconversion between $^3\pi, \pi^*$ IL and ^{3}MLCT states may exist when the two manifolds are in close energetic proximity [30,43,44]. A similar effect may be operating in metal containing polymers **P10–P50**.

2.6. Exciton diffusion and trapping by Re(I) chromophores

In order for the Re(I) sites to effectively quench the $^1\pi, \pi^*$ exciton, two processes must be rapid and efficient. (1) The exciton must diffuse rapidly along the polymer backbone, effectively sampling an entire polymer chain during its lifetime (≈ 1 ns). (2) The exciton must be trapped efficiently each time it comes within the encounter distance of a Re(I) repeat unit. If both processes are rapid and efficient, quenching is expected to be efficient even at low χ_{Re}. We now discuss background material pertinent to these two processes.

Several studies imply that intrachain diffusion of a $^1\pi, \pi^*$ exciton (process 1 above) in π-conjugated polymers is fast compared with its lifetime. For PPV-type polymer films, diffusion of "a relaxed exciton" (e.g. one that has already migrated from a short to a long conjugated segment by ultrafast Förster transfer) is thermally activated, and the one-dimensional diffusion length of the relaxed exciton is approximated to be 50 Å. Assuming that the data on PPV films can be extrapolated to the PPE-type polymers in solution, a 50 Å diffusion length implies that, during its lifetime, a $^1\pi, \pi^*$ exciton will sample 10 or more repeat units. Another study supports the notion that in PPE type π-conjugated polymers the $^1\pi, \pi^*$ exciton samples a substantial fraction of a polymer chain during its ca. 1 ns lifetime. Thus, Swager and co-workers demonstrated that an electron acceptor (paraquat) which is complexed to a cyclophane pendant group on a PPE-type polymer is extremely effective at quenching an exciton [14]. This work, albeit qualitative, implies that during its lifetime the $^1\pi, \pi^*$ exciton has a diffusion length comparable to the length of a typical polymer chain (20–30 repeat units in Swager's study).

The other important process for exciton quenching is the trapping event (process 2 above). A significant body of data on small-molecule transition metal complexes implies that this process should also be rapid and efficient in the metal–organic π-conjugated polymers. Thus, the fluorescence of organic ligands coordinated to d^6 transition metals is typically strongly quenched in small-molecule complexes [45]. For example, this effect is clearly manifest in complex **3**: free diimine ligand **2** is strongly fluorescent ($\Phi_{fl} \approx 1$); however, only very weak π, π^* IL fluorescence is observed from complex **3**. The IL fluorescence is quenched by intramolecular energy transfer to the MLCT manifold which is at lower energy compared with the IL state.

The experimental results on **P0–P50** imply that at room temperature in fluid solution the Re sites are not particularly efficient traps for the $^1\pi, \pi^*$ exciton. However, the median fluorescence lifetime $\langle\tau\rangle$ decreases as χ_{Re} increases, which is

consistent with a quenching mechanism that involves dynamic quenching of a diffusing exciton by the Re units. Unfortunately, the available data does not allow us to distinguish whether quenching is limited by exciton diffusion or exciton trapping by the metal complex sites. Given the large body of data on small molecule complexes which indicates that $^1\pi, \pi^*$ IL states are efficiently quenched by energy transfer to the MLCT manifold [45], we believe that the trapping event (process 2) should be very efficient in **P10–P50**. Thus, we tentatively conclude that the relatively inefficient quenching in the metal–organic polymers is a result of the slow intrachain diffusion of the $^1\pi, \pi^*$ exciton.

3. Experimental

3.1. Synthesis

Solvents and chemicals used for synthesis were of reagent grade and were used without purification unless otherwise noted. 5,5′-diethynyl-2,2′-bipyridine (**5**) was prepared from 5,5′-dibromo-2,2′-bipyridine (**4**) according to the method described by Ziessel and co-workers [33]. 2-Iodo-1,4-dimethoxybenzene (**6**) [46], 2,5-diiodo-1,4-dioctadecyloxybenzene (**9**) [14], and 4,4′-diethynylbiphenyl (**7**) [47] were prepared according to literature procedures. *fac*-(5,5′-diethynyl-2,2′-bipyridine)$Re^I(CO)_3Cl$ (**8**) was prepared by refluxing **5** with $Re(CO)_5Cl$ in toluene.

3.1.1. 5-Bromo-2-thiomethylpyridine [48]

2,5-Dibromopyridine (10.0 g, 42.2 mmol) was dissolved in DMF (200 ml) and the resulting solution was stirred under nitrogen. Sodium thiomethane (6.5 g, 92.8 mmol) was added to the DMF solution and the reaction was stirred at room temperature for 1 h. The resulting solution was rinsed with water (5 × 200 ml), extracted with diethyl ether, and the ether layer was separated and dried over sodium sulfate. After removal of the solvent under reduced pressure the crude product was obtained as a white crystalline solid. The crude product was purified by chromatography on silica gel (hexane solvent) and was obtained as a white crystalline material, yield 7.5 g (87%). ^{1}H-NMR ($CDCl_3$) δ2.52 (*s*, 3H), 7.0 (*d*, 1H), 7.56 (*dd*, 1H), 8.47 (*d*, 1H), ^{13}C-NMR ($CDCl_3$) δ 158.6, 150.1, 138.2, 122.6, 115.6, 13.4. Elemental analysis: calculated for C_6H_6NBrS: C, 35.31; H, 2.96; N, 6.86; found: C, 35.63; H, 2.89; N, 6.67.

3.1.2. 5-Bromo-2-methylsulphinylpyridine [35]

5-Bromo-2-thiomethylpyridine (7.2 g, 35.5 mmol) was dissolved in 45 ml of glacial acetic acid and hydrogen peroxide (4.80 g, 42.3 mmol) was then added dropwise to the solution. The reaction mixture was then stirred at room temeprature for 24 h at which time the mixture was cooled in an ice bath and neutralized with sodium carbonate until basic (pH = 12). The neutralized solution was extracted with diethyl ether, the ether layer was separated and dried over sodium sulfate. Evaporation of the ether under vacuum produced a white solid which was further purified by

chromatography on silica gel (hexane solvent), yield 7.30 g (94%) ^{1}H-NMR ($CDCl_3$) δ 2.75 (*s*, 3H), 7.85 (*d*, 1H), 8.0 (*dd*, 1H), 8.58 (*d*, 1H) ^{13}C-NMR ($CDCl_3$) δ 164.4, 150.4, 140.4, 121.8, 120.6, 41.0.

3.1.3. 5,5'-Dibromo-2,2'-bipyridine (4) [35]

n-Propyl magnesium bromide in THF (6.0 ml of a 1.0 M solution, 6.0 mmol) was added by using a syringe to an ice-cold, stirred solution of 5-bromo-2-methylsulphinylpyridine (1.90 g, 8.64 mmol) in 60 ml of diethylether. After addition of the Grignard reagent, the reaction mixture was allowed to warm to room temperature and stirred for 1 h. Water was then added and the reaction mixture was neutralized by the addition of dilute hydrochloric acid. The neutralized aqueous solution was extracted with toluene, the organic layers were combined and dried over sodium sulfate. After removal of solvents under reduced pressure, the crude product was rinsed with excess acetone and collected by filtration. After the acetone wash, the final product was obtained as a white solid, yield 0.66 g (49%). ^{1}H-NMR ($CDCl_3$) δ 7.92 (*dd*, 2H), 8.28 (*d*, 2H), 8.70 (*d*, 2H). ^{13}C-NMR ($CDCl_3$) δ 153.4, 150.0, 139.3, 122.0, 121.2.

3.1.4. 4,4'-bis-[(2,5-dimethoxyphenyl)ethynyl]biphenyl (1)

4,4'-Diethynylbiphenyl (**7**) (0.300 g, 1.48 mmol), 2-iodo-1,4-dimethoxybenzene (**6**) (0.820 g, 3.10 mmol), $Pd(PPh_3)_2Cl_2$ (0.063 g, 0.088 mmol) and CuI (0.034 g, 0.178 mmol) were placed in a 200 ml Schlenck flask that was purged with Argon. Tetrahydrofuran and diisopropylamine (8 and 5 ml, respectively) were added and the solution was heated at 70 °C for 10 h. Upon cooling, the reaction mixture was filtered to remove insoluble Pd-byproducts and the solvents removed in vacuo. The crude product was dissolved in CH_2Cl_2 and passed through a short (3 cm) column of silica gel, yielding an orange solid upon evaporation of the solvent, yield 0.586 g (84%). The material was purified further for spectroscopic studies by recrystallization from toluene; the compound was recovered after recrystallization as a light yellow solid, yield 0.420 g. ^{1}H-NMR ($CDCl_3$) δ 3.79, (*s*, 6H, OCH_3), 3.89 (*s*, 6H, OCH_3), 6.86 (*m*, 4H, phenyl), 7.08 (*d*, 2H, phenyl), 7.63 (*d*, 8H, biphenyl) ^{13}C-NMR ($CDCl_3$) δ 154.5, 153.2, 139.9, 132.1, 126.7, 118.0, 115.8, 112.9, 122.2, 93.2, 86.7, 56.5, 55.8.

3.1.5. 5,5'-bis[(2,5-dimethoxyphenyl)ethynyl]-2,2'-bipyridine (2)

5,5'-diethynyl-2,2'-bipyridine (**5**) (0.20 g, 0.98 mmol), 2-iodo-1,4-dimethoxybenzene (**6**) (0.562 g, 2.16 mmol) $Pd(PPh_3)_2Cl_2$ (41.2 mg, 0.058 mmol) and CuI (23 mg, 0.120 mmol) were placed in a 200 ml Schlenck flask that was purged with Argon. Tetrahydrofuran and diisopropylamine (8 and 5 ml, respectively) were added and the solution was heated at 70°C for 10 h, upon cooling the mixture was filtered and then the solvent removed in vacuo, yielding a brown solid. The crude product was purified for spectroscopic studies by preperative thin layer chromatography (silica gel, eluted with 2% $MeOH/CH_2Cl_2$). The purified product was obtained as a yellow solid, yield 75 mg. ^{1}H-NMR ($CDCl_3$) δ 3.80 (*s*, 6H, OCH_3), 3.90 (*s*, 6H, OCH_3), 6.90 (*m*, 4H, phenyl), 7.09 (*s*, 2H, phenyl), 7.98 (*d*, 2H, bpy, $J=7.8$ Hz),

8.40 (*br s*, 2H, bpy), 8.83 (*br s*, 2H, bpy) ^{13}C-NMR ($CDCl_3$) δ 154.6, 153.8, 153.2, 151.6, 139.4, 120.7, 120.5, 118,0, 116.5, 112.0, 90.2, 56.4, 55.8.

3.1.6. fac-(5,5'-bis[(2,5-dimethoxyphenyl)ethynyl]-2,2'-bipyridine)Re(CO)$_3$Cl (3)

Bipyridine **2** (0.050 g, 0.24 mmol) was dissolved in 10 ml of CH_2Cl_2/toluene (1:1 v:v) and the resulting solution was added to a 20 ml flask containing $Re(CO)_5Cl$ (0.217 g, 0.60 mmol). The reaction mixture was heated at reflux for 14 h. After this period the solution was cooled and the solvents removed in vacuo, yielding a crude orange solid. The product was purified by repeating rinsing with diethyl ether/toluene and was obtained as a brick orange solid, yield, 0.110 g (88%). ^{1}H-NMR ($CDCl_3$) δ 3.82 (*s*, 6H, OCH_3), 3.91 (*s*, 6H, OCH_3), 6.89 (*d*, 2H, phenyl), 6.96 (*d*, 2H, phenyl), 7.07 (*s*, 2H, phenyl), 8.10 (*br s*, 4H, bpy), 9.16 (*s*, 2H, bpy). ^{13}C-NMR ($CDCl_3$) δ 55.9, 56.3, 87.6, 94.9, 110.8, 112.0,, 117.9, 122.6, 124.6, 140.5, 153.0, 153.2, 155.1, 155.3, 196.7. HRMS (FAB, positive ion, NBA) calculated for $C_{33}H_{24}O_7N_2ReCl$ (M^+), 782.083, observed, 782.084; calculated for $C_{33}H_{24}O_7N_2Re$($M-Cl^+$), 747.114, observed, 747.112.

*3.1.7. Polymer **P0***

Diethynylbiphenyl **7** (44 mg, 0.220 mmol), diiododialkoxybenzene **9** (190 mg, 0.219 mmol) $PdCl_2$ (2 mg, 0.011 mmol), PPh_3 (13 mg, 0.0495 mmol) and CuI (2 mg, 0.011 mmol) were combined in 6 ml of diisopropylamine and 14 ml of THF under nitrogen. The mixture was heated at 70 °C for 16 h. Through the course of the polymerization the solution became noticeably more viscous and highly fluorescent (blue). The reaction mixture was cooled to room temperature and then added dropwise with stirring to 300 ml of acetone. The yellow precipitate was collected and washed repeatedly with hot acetone, hot acetonitrile, hot ethanol and hexane. Some lower molecular weight material was removed by the washings as evidenced by the fact that the washings were strongly fluorescent. After drying overnight at 40 °C, 130 mg of **P0** was isolated as a yellow solid, yield 73%. GPC ($CHCl_3$, polystyrene standards) M_n=13.5, M_w=37.4 kD (PDI=2.7). ^{1}H-NMR ($CDCl_3$) δ 0.87 (*br, t*), 1.24 (*br, s*), 1.56 (*br, m*), 1.84 (*br, m*), 4,04 (*br, t*), 6.92 (*br, s*), 7.0 (*br, s*), 7.62 (*br, s*). ^{13}C-NMR ($CDCl_3$) δ 14.1, 22.7, 26.1, 29.4, 29.7, 32.0, 69.7, 87.0, 94.8, 114.0, 116.9, 122.8, 126.8, 132.1, 140.0, 153.7.

*3.1.8. Polymer **P10***

Diethynylbiphenyl **7** (40 mg, 0.199 mmol), Re complex **8** (11 mg, 0.022 mmol), diiododialkoxybenzene **9** (190 mg, 0.219 mmol), $PdCl_2$ (2 mg, 0.011 mmol) PPh_3 (13 mg, 0.0495 mmol) and CuI (2 mg, 0.011 mmol) were combined in 6 ml of diisopropylamine and 14 ml of the THF under nitrogen. The mixture was heated at 70 °C for 16 h. Through the course of the polymerization the solution became noticeably more viscous and highly fluorescent (blue). The reaction mixture was cooled to room temperature and then added dropwise with stirring to 300 ml of acetone. The red-orange precipitate was collected and washed repeatedly with hot acetone, hot acetonitrile, hot ethanol and hexane. Some lower molecular weight material was removed by the washings as evidenced by fact that the washings were

strongly fluorescent. After drying overnight at 40 °C, 115 mg of P10 was isolated as a red-orange solid, yield 62%. GPC ($CHCl_3$, polystyrene standards) M_n=8.8, M_w=20.7 kD (PDI=2.3). ^{1}H-NMR ($CDCl_3$) δ 0.87 (*br*, *t*), 1.24 (*br*, *s*), 1.56 (*br*, *m*), 1.84 (*br*, *m*), 4.04 (*br*, *t*), 6.92 (*br*, *s*), 7.0 (*br*, *s*), 7.62 (*br*, *s*) 8.08 (*br*, *s*), 9.18 (*br*, *s*). ^{13}C-NMR ($CDCl_3$) δ 14.1, 22.7, 26.1, 29.4, 29.7, 32.0, 69.7, 87.0, 94.8, 114.0, 116.9, 122.8, 126.8, 132.1, 140.0, 153.7.

*3.1.9. Polymer **P25***

This polymer was prepared according to the procedure described for polymer **P10** except with 33 mg of **7** (0.166 mmol) and 28 mg of **8** (0.055 mmol). After purification **P25** was isolated as a red-brown solid, yield 115 mg (59 %). GPC ($CHCl_3$, polystyrene standards) M_n=7.9 kD, M_2=16.4 (PDI=2.1). ^{1}H-NMR ($CDCl_3$) δ 0.87 (*br*, *t*), 1.24 (*br*, *s*), 1.56 (*br*, *m*), 1.84 (*br*, *m*), 4.04 (*br*, *t*), 6.92 (*br*, *s*), 7.0 (*br*, *s*), 7.62 (*br*, *s*), 8.08 (*br*, *s*), 9.18 (*br*, *s*). ^{13}C-NMR ($CDCl_3$) δ 14.1, 22.7, 26.1, 29.4, 29.7, 32.0, 69.7, 87.0, 94.8, 114.0, 116.9, 122.8, 126.8, 132.1, 140.0, 153.7.

*3.1.10. Polymer **P50***

This polymer was prepared according to the procedure described for polymer **P10** except with 22 mg of **7** (0.11 mmol) and 56 mg of **8** (0.111 mmol). After purification, **P25** was isolated as a red-brown solid, yield 138 mg (65%). GPC ($CHCl_3$, polystyrene standards) M_n=7.8 kD, M_w=16.0 (PDI=2.0). ^{1}H-NMR ($CDCl_3$) 0.87 (*br*, *t*), 1.24 (*br*, *s*), 1.56 (*br*, *m*), 1.84 (*br*, *m*), 4.04 (*br*, *t*), 6.92 (*br*, *s*), 7.0 (*br*, *s*), 7.62 (*br*, *s*), 8.08 (*br*, *s*), 9.18 (*br*, *s*). ^{13}C-NMR ($CDCl_3$) δ 14.1, 22.7, 26.1, 29.4, 29.7, 32.0, 69.7, 87.0, 94.8, 114.0, 116.9, 122.8, 126.8, 132.1, 140.0, 153.7.

3.2. Photophysical measurements

All photophysical experiments were carried out using equipment and procedures that have been described in detail in previous publications [49,50]. Fluorescence quantum yields were determined relative to three actinometers (all in ethanol solution): anthracene (Φ_{fl}=0.27) [51], 9,10-dicyanoanthracene (Φ_{fl}=0.87) [52], and perylene (Φ_{fl}=0.87) [52]. The reported fluorescence quantum yields are the average of the experimentally determined quantum yields relative to the three actinometers.

Acknowledgements

We gratefully acknowledge the National Science Foundation for support of this work (Grant No. CHE-9401620).

References

[1] A.O. Patil, A.J. Heeger, F. Wudl, Chem. Rev. 88 (1988) 183.
[2] T.A. Skotheim (Ed.), Handbook of Conducting Polymers, Parts 1 and 2, Marcel-Dekker, New York, 1986.

[3] G.A. Sotzing, J.R. Reynolds, P.J. Steel, Chem. Mater. 8 (1996) 882.
[4] A.P. Davey, S. Elliott, O. O'Connor, W. Blau, J. Chem. Soc. Chem. Comm. (1995) 1433.
[5] F.L. Carter (Ed.), Molecular Electronic Devices, Marcel-Dekker, New York, 1982.
[6] F.L. Carter (Ed.), Molecular Electronic Devices II, Marcel-Dekker, New York, 1986.
[7] W.E. Moerner, S.M. Silence, Chem. Rev. 94 (1994) 127.
[8] J.H. Burroughes, D.D.C. Bradley, A.R. Brown, R.N. Marks, K. Mackay, R.H. Friend, P.L. Burn, A.B. Holmes, Nature 347 (1990) 539.
[9] D.R. Baigent, P.J. Hamer, R.H. Friend, S.C. Moratti, A.B. Holmes, Synth. Meth. 71 (1995) 2175.
[10] G. Green, G. Leditzky, B. Ullrich, G. Leising, Adv. Mater. 4 (1992) 36.
[11] N.C. Greenham, A.R. Brown, D.D.C. Bradley, R.H. Friend, Synth. Meth. 555657 (1993) 4134.
[12] D. Dagani, Chemical and Engineering News, March 4th issue (1996) 22.
[13] T.M. Swager, C.J. Gil, M.S. Wrighton, J. Phys. Chem. 99 (1995) 4886.
[14] Q. Zhou, T.M. Swager, J. Am. Chem. Soc. 117 (1995) 12593.
[15] M. Moroni, J. LeMoigne, S. Luzzati, Macromolecules 27 (1994) 562.
[16] P. Wautelet, M. Moroni, L. Oswald, J. LeMoigne, A. Pham, J.-Y. Bigot, Macromolecules 29 (1996) 446.
[17] L.J. Rothberg, M. Yan, F. Papadimitrakopoulos, M.E. Galvin, E.W. Kwock, T.M. Mille, Synth. Meth. 80 (1996) 41.
[18] B. Xu, S. Holdcroft, Adv. Mater. 6 (1994) 325.
[19] R.D. Scurlock, B. Wang, P.R. Ogilby, J.R. Sheats, R.L. Clough, J. Am. Chem. Soc. 117 (1995) 10194.
[20] B. Wang, M.R. Wasielewski, J. Am. Chem. Soc. 119 (1997) 12.
[21] T. Maruyama, T. Yamamoto, Synth. Meth. 69 (1995) 553.
[22] S.C. Rasmussen, D.W. Thompson, V. Singh, J.D. Petersen, Inorg. Chem. 35 (1996) 3449.
[23] Z. Peng, L. Yu, J. Am. Chem. Soc. 118 (1996) 3777.
[24] Z. Peng, A.R. Gharavi, L. Yu, J. Am. Chem. Soc. 119 (1997) 4622.
[25] T.J. Meyer, Prog. Inorg. Chem. 30 (1983) 389.
[26] A. Juris, V. Balzani, F. Barigelletti, S. Campagna, P. Belser, A. von Zelewsky, Coord. Chem. Rev. 84 (1988) 85.
[27] K.S. Schanze, D.B. MacQueen, T.A. Perkins, L.A. Cabana, Coord. Chem. Rev. 122 (1993) 63.
[28] K.D. Ley, C.E. Whittle, M.D. Bartberger, K.S. Schanze, J. Am. Chem. Soc. 119 (1997) 3423.
[29] L.A. Worl, R. Duesing, P. Chen, L. Della Ciana, T.J. Meyer, J. Chem. Soc., Dalton Trans. (1991) 849.
[30] L.A. Sacksteder, M. Lee, J.N. Demas, B.A. DeGraff, J. Am. Chem. Soc. 115 (1993) 8230.
[31] A.D. Schluter, G. Wegner, Acta Polym. 44 (1993) 59.
[32] R.F. Heck, Palladium Reagents in Organic Synthesis, Academic Press, Orlando, FL, 1985.
[33] F.M. Romero, R. Ziessel, Tetrahedron Lett. 35 (1994) 9203.
[34] F.M. Romero, R. Ziessel, Tetrahedron Lett. 36 (1995) 6471.
[35] S. Oae, T. Kawai, N. Furukawa, Phosph. Sulf. 34 (1987) 123.
[36] H.J. Rader, J. Spickerman, M. Kreyenschmidt, K. Mullen, Macromol. Chem. Phys. 197 (1996) 3285.
[37] G. Odian, Principles of Polymerization, 3rd ed., Wiley-Interscience, New York, 1991.
[38] D.R. Gamelin, M.W. George, P. Glynn, F.-W. Grevels, F.P.A. Johnson, W. Klotzbücher, S.L. Morrison, G. Russell, K. Schaffner, J.J. Turner, Inorg. Chem. 33 (1994) 3246.
[39] S.L. Murov, I. Carmichael, G.L. Hug, Handbook of Photochemistry, 2nd ed., Marcel-Dekker, New York, 1993.
[40] R.S. Lumpkin, T.J. Meyer, J. Phys. Chem. 90 (1986) 5307.
[41] T.G. Kotch, A.J. Lees, S.J. Fuerniss, K.I. Papathomas, R.W. Snyder, Inorg. Chem. 32 (1993) 2570.
[42] H.F. Wittman, K. Fuhrmann, R.H. Friend, M.S. Khan, J. Lewis, Synth. Meth. 555657 (1993) 56.
[43] J.A. Burt, G.A. Crosby, Chem. Phys. Lett. 220 (1994) 493.
[44] D.R. Striplin, G.A. Crosby, Inorg. Chem. (submitted).
[45] A.J. Lees, Chem. Rev. 87 (1987) 711.
[46] A. Manoucher, T. Wallace, Tetrahedron 44 (1988) 5939.
[47] M. Wright, Macromolecules 22 (1989) 3256.
[48] L. Testaferri, M. Tiecco, M. Tirgoli, D. Bartoli, A. Massoli, Tetrahedron 41 (1985) 1373.
[49] Y. Wang, K.S. Schanze, Chem. Phys. 176 (1993) 305.
[50] Y. Wang, K.S. Schanze, Inorg. Chem. 33 (1994) 1354.
[51] W.R. Dawson, M.W. Windsor, J. Phys. Chem. 72 (1968) 3251.
[52] W.R. Ware, W. Rothman, Chem. Phys. Lett 39 (1976) 449.